The [10-10] edge dislocation in the wurtzite structure: A high-resolution transmission electron microscopy investigation of [0001] tilt grain boundaries in GaN and ZnO

Siqian Li, Jun Chen, Pierre Ruterana

The $[10\bar{1}0]$ edge dislocation in the wurtzite structure: A high-resolution transmission electron microscopy investigation of [0001] tilt grain boundaries in GaN and ZnO

Siqian Li [a*], Jun Chen [a] and Pierre Ruterana [a]

[a] *CIMAP UMR 6252 CNRS, ENSICAEN, UNICAEN and CEA, 6, Boulevard du Maréchal Juin, 14050 Caen Cedex, France*

* Corresponding author.
E-mail addresses: siqian.li@ensicaen.fr (Siqian Li), jun.chen@unicaen.fr (Jun Chen), pierre.ruterana@ensicaen.fr (Pierre. Ruterana).

Abstract

A detailed topological analysis and atomic structure investigation of [0001] tilt grain boundaries (GBs) in GaN and ZnO has been carried out using atomistic simulation and high-resolution transmission electron microscopy (TEM). The analysis of Σ7 asymmetric GBs in GaN, shows that they are only made of well-separated $\mathbf{a} = \frac{1}{3} < 11\bar{2}0 >$ edge dislocations based on the three basic structural units: 4-, 8- and 57-atom rings. In this compound, the Burgers vectors adapt their orientations in order to accommodate the rotation angle of the grain boundary. However, in ZnO, the topology of such GBs is shown to comprise two types of dislocation contents: one of them follows the behaviour of GaN in which individual **a** edge dislocations are dominant; the second is the $[10\bar{1}0]$ edge dislocation which comes out as a distinct structural with a large core as pointed out in the Σ13 (27.8°/32.2°) GBs. The determined low-energy configuration of this $[10\bar{1}0]$ dislocation is made of connected 4-8-6-atom rings in agreement with an early proposal of its possible geometrical model. The investigation of electronic structure these GB dislocations shows the evidence of a deep state induced above the valence band edge in all the structural units comprising the 57-atom ring. In contrast to previous reports which solely ascribed such states to dangling bonds, this one is ascribed to the cooperative effect of Zn-Zn wrong bonds and broken O-O bonds inside the 57-atomic ring.

Keywords: Grain boundaries; Wurtzite; $[10\bar{1}0]$ edge dislocations; Structural units; High-resolution TEM.

1. Introduction

A critical role is played by polycrystalline materials of technological importance where the physical and functional performance of the corresponding devices is governed by the atomic structures of GBs [1]. The corresponding research has led to the development of the structural unit model which describes the GB atomic structure versus the macroscopic degrees of freedom (tilt, rotation, interface, ...) [2-4]. In this formalism, GBs are constructed by a few fundamental bricks, known as the "structural units". A typical example can be seen in [110] tilt GB of cubic Al metal that has been described by the combination of a limited number of structural unit models [4].

During the last years, many attempts have been made in order to extend this structural unit concept to the GB investigation of lower symmetric systems like wurtzite structure. Especially along with the development of light-emitting devices, wide bandgap semiconductors of GaN and ZnO attract a great attention due to their excellent performance in luminescence properties. The electronically activated states which may be induced by the GBs themselves or by the interfacial complexes from the interaction between GBs and native defects, such as intrinsic point defects [5,6] and impurities [7], can greatly affect the functionality of related devices, which is a strong motivation for their investigations.

Topological analysis has been performed by constructing the coincidence site lattice (CSL) in wurtzite symmetry at a certain rotation angle. It is widely accepted that the atomic structures of the high angle (>15°) GBs are made of bulk dislocation-like structural units [8,9]. For instance in GaN, it was shown through investigation combining high-resolution TEM and multiscale atomic modelling, that three configurations of pure $\mathbf{a} = \frac{1}{3} < 11\bar{2}0 >$ edge threading dislocations are the structural units of [0001] tilt GBs: exhibiting, respectively, 4-, 57- and 8-atom rings [5-6, 10-13]. They form upon growth of GaN on the six or three fold symmetry surfaces of highly mismatched substrates [14-17]. Similarly, in the work of Oba et al. [8] and our previous reports [18], an array of dislocation-like units in Σ7 [0001] GBs were observed which also validates the concept of dislocation core as structural units in ZnO GBs.

In this study, we report a detailed investigation of the [0001] tilt GBs in wurtzite GaN and ZnO with a close combination of atom-scale TEM and topological analysis. We demonstrate that, in wurtzite symmetry, the primary GB dislocations are only made of two contents: $\mathbf{a} = \frac{1}{3} < 11\bar{2}0 >$ and $[10\bar{1}0]$ edge dislocations. To begin with, we propose that the topological

description of the GB (boundary indices, CSL scheme and dislocation identification) should be the starting point for a better characterization and theoretical modelling, seen as section II. Section III gives the experimental details and computational procedures. In section IV, detailed investigations on Σ7 and Σ13 [0001] GBs in GaN and ZnO are provided to gain insight into the structural difference between GaN and ZnO. Furthermore, the electronic properties of the GB structures are discussed in section V. The aim of this work is to understand the local structures of GBs in GaN and ZnO, as well as the role of the GB dislocations in the electronic properties of materials and on the technological applications.

2. Topological analysis of GBs in wurtzite symmetry

Pond and coworkers [19-20] have developed an elegant device called the "topological theory" for the description of GBs. They have proposed the use of dichromatic complex to lay out two crystals related by their respective orientation: represented in white (λ) and black (μ) [19]. This allows to visually obtain, for some special misorientation (Σ), the three-dimensional CSLs. In case of wurtzite symmetry and rotation axis of around the [0001], the CSLs resulting from rotation angles of θ and 60°-θ are identical except for a translocation of c/2 [20]. The side and diagonal of the CSL constitute the densest boundary planes named as GB which can be shared by the two adjacent grains. Therefore, complying with the principle of minimum energy, only limited boundary planes tend to form as the most stable GB configurations [9,21]. More specifically, in Pond's formulation, a GB is considered as a particular defect which is completely defined by the boundary plane indices (side or diagonal of the CSL) and its corresponding Burgers vector in one period of this boundary which connects the two nearest-neighbour coincident sites. Following this definition, the nearest-neighbour common sites are connected by a crystallographic defect known as a GB defect which, in most case, corresponds to one or more elemental dislocations of the parent crystal [22] whose strain field overlap and release the misorientation between the grains. The determination of the defect content follows the conventional Burgers circuit that runs in the two adjacent crystals, enclosing one period of the boundary plane. After mapping this circuit into one of the reference crystals (λ or μ), the resulting closure failure is the Burgers vector of the particular GB dislocation [22].

The typical case of Σ7 (21.79°/38.21°) [0001] tilt GBs are shown in Fig. 1. Considering first the rotation angle of θ=21.79° in Fig. 1(a), the unit cell of the obtained CSL is identified as ABSX. The boundary indices of the side and the diagonal of the CSL, which are the

locations of GBs, are: $\{1/3[\bar{1},5,\bar{4},0]/(\bar{3},1,2,0)\}$ and $\{[2,\bar{3},1,0]/(\bar{4},\bar{1},5,0)\}$. For the side of the CSL, the defect content per period of the GB is determined by drawing the Burgers circuit from site S to X in λ crystal ($C_\lambda = \mathbf{a}_3 - 2\mathbf{a}_2$, red), and the from X to F in μ crystal($C_\mu = -2\mathbf{a}_3 + \mathbf{a}_2$, blue), which encloses one period of SCL in the boundary plane. After mapping this circuit SXF in λ crystal (red circuit in Fig.1(a)), the closure failure pointing from F to S is the defect content (Burgers vector) that corresponds to FS=$-\mathbf{a}_{1\lambda}$. When a similar circuit is drawn around one period of the diagonal of the CSL $\{[2,\bar{3},1,0]/(\bar{4},\bar{1},5,0)\}$, the obtained defect content comes out as F'S'=$(\mathbf{a}_3 - \mathbf{a}_1)_\lambda$, which corresponds to a $[10\bar{1}0]$ dislocation. Similarly, for Σ7 at θ=38.21° (Fig. 1(b)), a $[10\bar{1}0]$ dislocation $(\mathbf{a}_2 - \mathbf{a}_1)_\lambda$ and a $-3\mathbf{a}_{1_\lambda}$ dislocation are obtained along the side $\{1/3[1,4,\bar{5},0]/(\bar{3},2,1,0)\}$ and the diagonal $\{[\bar{1},3,\bar{2},0]/(\bar{5},1,4,0)\}$ of CSL, respectively.

Similar analysis applied for Σ13 [0001] GBs is shown in Fig. 2. As can be seen, at the rotation angle of 27.8° (Fig. 2(a)), the defect contents along the side $\{1/3[2,5,\bar{7},0]/(\bar{4},3,1,0)\}$ and the diagonal $\{1/3[\bar{2},4,\bar{3},0]/(\bar{7},2,5,0)\}$ of CSL exhibit identical Burgers vectors in comparison with Σ7 38.21° GB, which are $(\mathbf{a}_2 - \mathbf{a}_1)_\lambda$ and $-3\mathbf{a}_{1_\lambda}$, respectively. However, things are different in the case of Σ13 32.2° GB. As can be seen in Fig. 2(b), defect content with a Burgers vector of $-2\mathbf{a}_{1_\lambda}$ is revealed along the side $\{1/3[\bar{2},7,\bar{5},0]/(\bar{4},1,3,0)\}$ of the CSL. As for the diagonal $\{[\bar{3},4,\bar{1},0]/(\bar{5},\bar{2},7,0)\}$ of the SCL, a larger Burgers vector of $2(\mathbf{a}_3 - \mathbf{a}_1)_\lambda$ is seen to be the defect content of this GB.

More extensively, in addition to the Σ7 and Σ13 GBs described above, the main CSLs of [0001] tilt GBs can be systematically generated in wurtzite crystal with rotation angles up to 60°. As reported in Table I all the GBs are made of $\mathbf{a} = \frac{1}{3} < \bar{2},1,1,0 >$ and $[1,0,\bar{1},0]$ dislocations whose number increases mainly with the length of the corresponding boundary plane period. We may have large Burgers vector up to -9$\mathbf{a}_1$ along the diagonal $\{[3,\bar{8},5,0]/(\overline{13},2,11,0)\}$ of CSL in Σ49 43.57° GB and $4[1,0,\bar{1},0]$ for the diagonal plane $\{[5,\bar{6},1,0]/(\bar{7},\bar{4},11,0)\}$ for Σ31 42.10° GB. Therefore, from this analysis it comes out that the $[10\bar{1}0]$ dislocation is one of the two structural units which should basically contribute to the construction of the [0001] tilt GBs in the wurtzite symmetry.

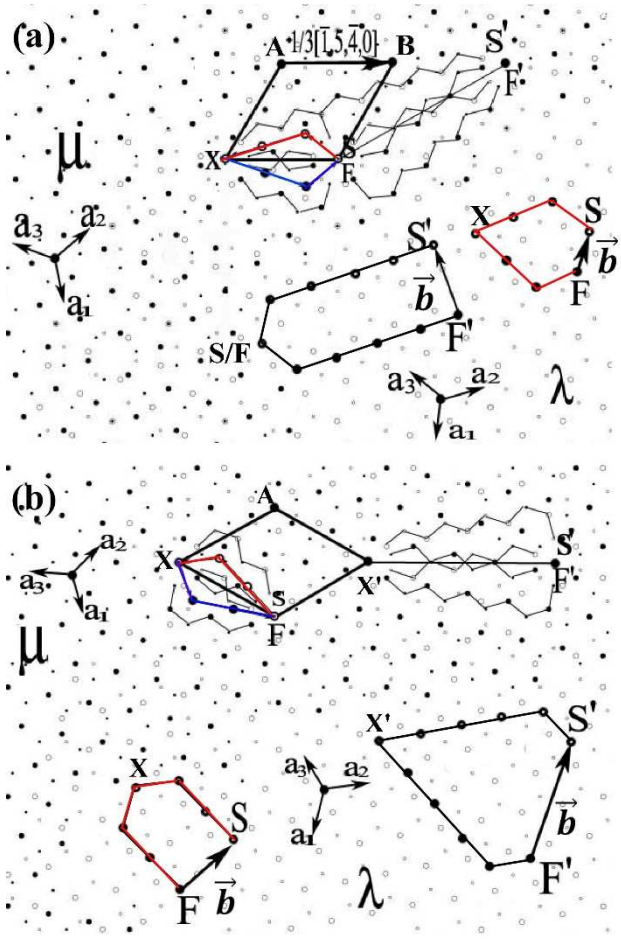

Fig. 1. Dichromatic complexes and Burgers circuits of Σ7 GBs. In each CSL, the unit cell is underlined as ABSX and AX'FX. Burgers circuits are drawn around one period of the boundary plane for the side and the diagonal of CSL, and after mapping in λ crystal, the defect contents (Burgers vectors, marked as $\vec{b}$) are shown as the vector connecting the final and starting sites for the side (FS) and diagonal (F'S'), respectively. Red and blue lines represent the circuits in λ and μ crystals. The grey and black marks stand for the λ or μ crystal, respectively. The rotation angle of the GBs is (a) θ=21.79° and (b) θ=38.21°

Following the work of Hornstra [23] in the diamond structure, Osipiyan and Smirnova [24] presented a detailed geometrical investigation of the perfect dislocations that may form in the wurtzite lattice. Apart from the straightforward four dislocations which possess the two translations of $1/3<11\bar{2}0>$ and $<0001>$ as the Burgers vectors, the authors suggested additional 9 different dislocations as well. Two of the set exhibit a Burgers vector of $<1\bar{1}00>$ type and a glide plane of $\{11\bar{2}0\}$: the first is of pure edge with its dislocation line along $[0001]$ direction, whereas the second one is of mixed type with the dislocation line along $<\bar{1}101>$. Of particular interest is the edge type one that may form as threading dislocation during the growth of layers along the conventional [0001] growth direction for wurtzite materials. Indeed, experimental studies have clearly shown that it can be one of the structural

unit to form the [0001] tilt GBs [12]. In the case of GaN, it was shown that the periodic boundaries such as symmetric Σ19, Σ7 and Σ13 GBs [5] can be explained in terms of a mixture of the three basic structural units of $\mathbf{a} = \frac{1}{3}[11\bar{2}0]$ dislocation [8,18,25]. As for ZnO, a straight 5757-atom ring core structure was reported in Σ13 GB in correlation between TEM observation and atomistic modelling [18].

Therefore, the question is to determine the atomic structure of GBs formed by the topologically expected $[10\bar{1}0]$ dislocation in the wurtzite crystals. In the following section, the atomic structures of Σ7 and Σ13 GBs are discussed with a specific focus on the $[10\bar{1}0]$ edge dislocation structural unit through a close combination of high-resolution TEM and atomistic modelling in GaN and ZnO.

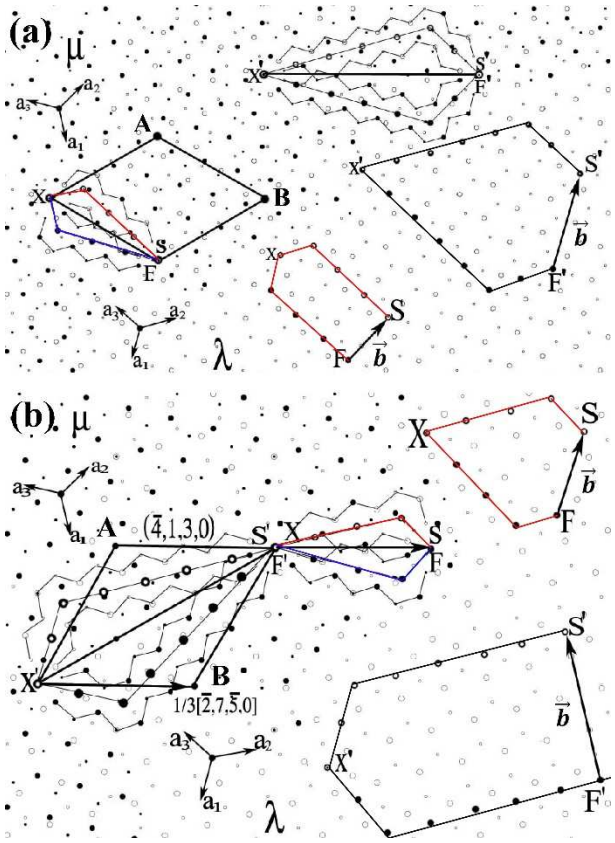

Fig. 2. Dichromatic complexes of Σ13 GBs at rotation angles of (a) θ=27.8° and (b) θ=32.3°. Image description follows the same way in Fig.1.

Table 1

Burgers vectors of interface dislocations of the main [0001] tilt GBs in wurtzite.

GB Parameters				Primary dislocation content	
	Tilt (°)	Boundary Plan	Period	Vector	Length
19	13.70	$(\bar{5},2,3,0)$	1/3 $[\bar{7},\bar{1},8,0]$	$-\mathbf{a}_1$	1/3 $[\bar{2},1,1,0]$
		$(\bar{7},\bar{1},8,0)$	$[\bar{3},5,\bar{2},0]$	$\mathbf{a}_1-\mathbf{a}_3$	$[1,0,\bar{1},0]$
	46.83	$(\bar{5},3,2,0)$	$1/3[1,7,\bar{8},0]$	$2(\mathbf{a}_2-\mathbf{a}_1)$	$2[\bar{1},1,0,0]$
		$(\bar{8},1,7,0)$	$[3,\bar{5},2,0]$	$-6\mathbf{a}_1$	2 $[\bar{2},1,1,0]$
49	16.43	$(\bar{8},3,5,0)$	$1/3[\bar{2},13,\bar{11},0]$	$-2\mathbf{a}_1$	2/3 $[\bar{2},1,1,0]$
		$(\bar{11},\bar{2},13,0)$	$[5,\bar{8},3,0]$	$2(\mathbf{a}_3-\mathbf{a}_1)$	$2[\bar{1},0,1,0]$
	43.57	$(\bar{8},5,3,0)$	$1/3[2,11,\bar{13},0]$	$3(\mathbf{a}_2-\mathbf{a}_1)$	$3[\bar{1},1,0,0]$
		$(\bar{13},2,11,0)$	$[3,\bar{8},5,0]$	$-9\mathbf{a}_1$	3 $[\bar{2},1,1,0]$
31	17.90	$(\bar{6},5,1,0)$	$1/3[4,7,\bar{11},0]$	$\mathbf{a}_1-\mathbf{a}_2$	$[1,\bar{1},0,0]$
		$(\bar{11},4,7,0)$	$[\bar{1},6,\bar{5},0]$	$-3\mathbf{a}_1$	$[\bar{2},1,1,0]$
	42.10	$(\bar{6},1,5,0)$	$1/3[\bar{4},11,\bar{7},0]$	$-4\mathbf{a}_1$	4/3 $[\bar{2},1,1,0]$
		$(\bar{7},\bar{4},11,0)$	$[5,\bar{6},1,0]$	$4(\mathbf{a}_3-\mathbf{a}_1)$	$4[\bar{1},0,1,0]$
7	21.79	$(\bar{3},1,2,0)$	$1/3[\bar{1},5,\bar{4},0]$	$-\mathbf{a}_1$	1/3 $[\bar{2},1,1,0]$
		$(\bar{4},\bar{1},5,0)$	$[2,\bar{3},1,0]$	$\mathbf{a}_3-\mathbf{a}_1$	$[\bar{1},0,1,0]$
	38.21	$(\bar{3},2,1,0)$	$1/3[1,4,\bar{5},0]$	$\mathbf{a}_2-\mathbf{a}_1$	$[\bar{1},1,0,0]$
		$(\bar{5},1,4,0)$	$[\bar{1},3,\bar{2},0]$	$-3\mathbf{a}_1$	$[\bar{2},1,1,0]$
13	27.80	$(\bar{4},3,1,0)$	1/3 $[2,5,\bar{7},0]$	$\mathbf{a}_2-\mathbf{a}_1$	$[\bar{1},1,0,0]$
		$(\bar{7},2,5,0)$	$[\bar{1},4,\bar{3},0]$	$-3\mathbf{a}_1$	$[\bar{2},1,1,0]$
	32.20	$(\bar{4},1,3,0)$	1/3 $[\bar{2},7,\bar{5},0]$	$-2\mathbf{a}_1$	2/3$[\bar{2},1,1,0]$
		$(\bar{5},\bar{2},7,0)$	$[\bar{3},4,\bar{1},0]$	$2(\mathbf{a}_2-\mathbf{a}_1)$	$2[\bar{1},0,1,0]$

3. Methodology

3.1. Experimental procedures

ZnO layers have been deposited on (0001) sapphire between 550 °C and 650 °C using magnetron sputtering. A radio frequency (RF) power of 150 W was used for ZnO deposition. Before the actual deposition, the ZnO target was subjected to a pre-sputter step for 5 minutes to remove contaminations from the surface. The as-deposited films were annealed at 850 ℃ for 1 hour at ambient atmosphere which is designed to improve the crystalline quality. In early reports GaN layers grown by molecular beam epitaxy have been used to investigate

[0001] tilt GBs [5]. In this work, we shall particularly discuss the results obtained on Σ7 asymmetric GBs in GaN for comparison to the ZnO case.

The TEM specimens were mechanically polished down to 100 μm and then dimpled to 10 μm from back surface. The electron transparency was finally obtained by ion-milling with the sample holder maintained at liquid nitrogen temperature in order to minimize the ion beam damage. The experimental observations were carried out in a 002B Topcon high-resolution TEM operated at 200 kV with a point to point resolution of 1.8Å. The image simulation based on multislice method was carried out using the electron microscopy software [26,27].

3.2. Computational details

The atomistic simulation methodology was performed in two steps; first within molecular dynamics based on our modified Stillinger-Weber (SW) empirical potentials [28,29] and second with ab initio techniques in order to determine the electronic structure of the GBs. The modified SW empirical potential takes only into account the two- and three- body short-range interactions so that it can handle very large systems with low computing cost. The SW parameters for Zn-O were optimized by fitting the structural parameters and the elastic constants to the experimental results. As the treatment of semiconductor compounds raises the problem of wrong bonds, which form in crystallographic defects, for the Zn-Zn and O-O parameters, we fitted the formation energy calculation of inversion domain boundaries (IDBs: Holt IDB and IDB*) which contain wrong bonds to the results of Yanfa et al. through ab-initio calculation [30]. At the end, the obtained formation energy of IDB* reaches to 0.4 eV, which coincides with the first principle calculations [30]. For constructing the GBs, all possible distinct initial crystallographic configurations have been considered for a given interface and the three-dimensional periodic boundary conditions were used. In each case, the corresponding γ surface (energetic minima) of each starting configuration has been addressed by taking into account the translations in two directions: parallel to the tilt axis ([0001] direction) and to boundary plane, respectively. Atoms are fully relaxed in the third direction which is normal to the boundary plane [25].

The first principle calculation was carried out using the SIESTA package [31] with a self-interaction correction (SIC) scheme for LDA as exchange correlation parametrized by Perdew and Zunger [32] and the standard norm-conserving pseudopotentials for Zn and O were used

for the core-valence electron interactions. The energy cutoff was set to 250 Ry and the k-point in Brillouin zone was sampled in 4×4×4 Monkhorst-Pack scheme.

We follow the definition of formation energy for boundary in periodic boundary conditions as proposed by Northrup et al [33]:

$$\sigma_{wall} = \frac{1/2\,(E - E_{bulk})}{A}$$

where $1/2\,(E - E_{bulk})$ is the formation energy of a single boundary by subtracting the total energy (E_{bulk}) of a bulk structure from the total energy (E) of the supercell containing two equivalent GBs. The factor of *A* is the area of the periodic unit cell of the boundary plane.

4. Atomic structure of the $[10\bar{1}0]$ edge dislocation

4.1. Energetics of the three basic structural units

As already has been reported [9,25,34], three basic structure units (4-, 8-, 57-atom rings) may be considered as the primitive bricks for constructing the [0001] tilt GBs in the wurtzite structure. However, the energetic stability competition of these structures depends not only on the crystallographic geometry but also on the elements forming the compounds. Therefore, it is necessary to determine the energetic difference of these three basic structural units for instance between GaN and ZnO.

In the simplest case, Σ7 GB based on the each of three basic structure units is taken as the example to explain the different behavior of ZnO and GaN. Table II shows the calculated formation energies of the Σ7 ZnO GBs which are made of the three basic structural units using SW potentials and first-principle calculation. The energies with SW(O) are calculated in open-core condition without considering (wrong bonds or long bonds) inside the dislocation core. The Zn-Zn, O-O wrong bonds and Zn-O long bonds are counted in the condition of closed-core named as SW(C). As can be seen, the formation energies are sensitive to the conditions used for calculation and the 57- configuration always appears to have a higher energy in all the calculations. This energy trend is at variance from the case of GaN [9] in which 57- structural unit has been reported to always exhibit the lowest energy. However it is in agreement with the relative stability of ZnO GBs calculated by J. Y. Roh et al. [35]. This may be explained by the energetically unfavorable Zn-Zn and O-O wrong bonds formed at 57-atom rings which may theoretically not be expected in this more ionic material.

Table 2

Formation energies of the Σ7 21.79° GBs formed by the three basic structural units in ZnO. The energies are given in mJ/m^2.

Dislocation core	SW (O)	SW(C)	SIESTA
4-	1174	1174	1078
8-	1071	1347	999
57-	1616	1447	1276

4.2. The $[10\bar{1}0]$ edge dislocation in GaN

In GaN specimens, an asymmetric boundary has been observed with a rotation angle of 38.21°, which agrees with the Σ7 GB in CSL notation. As per Fig. 3(a) where 3 periods were marked, Burgers circuit SXF mapping determined a dislocation content of -2$\mathbf{a}_1$+$\mathbf{a}_2$ in one period. In this figure, an interfacial step is clearly visible to connect V and X, indeed as period 3 of the grain boundary is shifted upward. And thus the boundary plane is characterized as $(\bar{3}8\bar{5}0)_\lambda/(0\bar{1}10)_\mu$, rather than the as would be expected $[\bar{1},3,\bar{2},0]/(\bar{5},1,4,0)$ for a symmetric grain boundary with a theoretical dislocation content of -3$\mathbf{a}_1$. In order to further clarify its atomic structure, the GB has been reconstructed and the dislocation cores exhibit a mixture of the three structural units of the $\frac{1}{3}[11\bar{2}0]$ edge dislocations, as seen in the superimposed atom cycles in Fig. 3(a). A closer examination in Fig. 3(b) shows that both period 1 and 2 are made of two 57- and one 8-atom rings with a total dislocation content of -2$\mathbf{a}_1$+$\mathbf{a}_2$. However, in period 1, one 57-atom ring is close to the 8- atom ring neighbor and both sum up to form a dislocation element of $[\bar{1}100]$. In the same period, the other 57-atom ring lies slightly at a distance so that the total dislocation content is exactly -$\mathbf{a}_1$+$[\bar{1}100]$. In contrast, two 57-atom rings are incorporated as the <$10\bar{1}0$> edge dislocation in period 2. Similar results have also obtained in GaN for Σ7 21.79° asymmetric GB, in which 4-atom ring was involved [5]. This means that, $[10\bar{1}0]$ edge dislocation in GaN GB can be arbitrarily formed by two of the three **a** edge dislocations. Therefore, in GaN, the [0001] tilt GBs can be constructed as the combination of the only three individual **a** edge dislocations with their Burgers vectors rotated in order to accommodate the dislocation content.

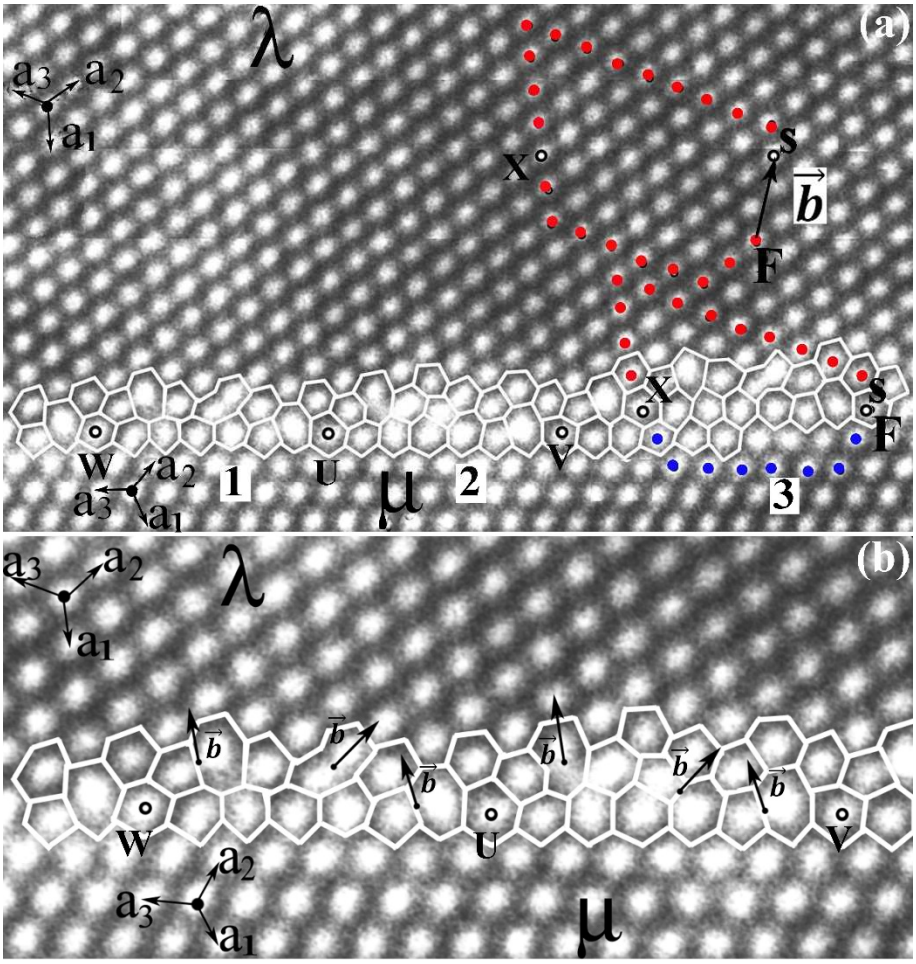

Fig. 3. (a) A Σ7 38.21° asymmetric GB exhibiting 3 periods (period 1: WU, period 2: UV, period 3: XS) along the boundary plane which are made of the $[11\bar{2}0]$ edge dislocation cores. Small open circles mark GB periods and are named as W, U, V, X, S/F. An interfacial step between the V and X is present. The Burgers circuit of period 3 goes from the S to X in λ crystal (red), and it goes from X to the F in μ crystal (blue). This Burgers circuit mapped in λ crystal then presents the closure failure FS or defect content of the grain boundary period which corresponds to the Burgers vector $\vec{b}$. (b) In each period, the Burgers vectors $\vec{b}$ of the primary dislocations rotate their directions in order to accommodate the defect content. The arrows show the directions of these primary grain boundary dislocations.

4.3. The $[10\bar{1}0]$ edge dislocation in ZnO

As reported in Ref. 18, we have successfully achieved the co-existence of two epitaxial relationships in ZnO layer based on sapphire: $[11\bar{2}0]_{ZnO}//[10\bar{1}0]_{Sap}$ and $[10\bar{1}0]_{ZnO}//[10\bar{1}0]_{Sap}$. Besides, the average rotation angle measured deviation as can be seen in the elongated shape of diffraction spots (Fig. 5 of Ref. 18). In order to fit the growth orientation of the domains, one would expect a formation of Σ97 GBs whose theoretical rotation angles are 29.41°/30.60°, which are the coincidence orientation closest to 30° [9]. However, during all the subsequent analysis in high-resolution TEM, we only observed Σ13 (27.80°/32.20°) GBs

in these samples. Moreover, the topological investigation of CSLs does not show a Burgers vector of 5**a** which is supposed to be the dislocation content of Σ97 GB.

Figure 4(a) shows the high-resolution TEM micrograph of the observed Σ13 GB with a certain rotation angle, which comprises two periodic boundary planes (the side and diagonal of the corresponding CSL). The symmetric boundary plane indices are first determined along the corresponding periods. Subsequently the defect contents are specified by mapping the Burgers circuit SXF in λ crystal, shown as C1 and C2. The corresponding Burgers vectors are ($\mathbf{a}_2$-$\mathbf{a}_1$) and (-3$\mathbf{a}_1$) for the side $\{\frac{1}{3}[2,5,\bar{7},0]/(\bar{4},3,1,0)\}$ and diagonal $\{[\bar{4},3,1,0]/(\bar{7},2,5,0)\}$ of SCL, respectively. When referring to the topological CSL diagram in Fig. 4(b) and dichromatic complex in Fig. 2, this exactly points out a Σ13 GB with a rotation angle of 27.8° around [0001] axis. In addition, as shown in Fig. 4(a), the atomic structure of the defect inside the boundary plane $(\bar{4},3,1,0)$, side of the CSL, clearly exhibits a large white contract which corresponds to a dislocation element of $\frac{1}{3}[\bar{1},2,\bar{1},0]-\frac{1}{3}[2,\bar{1},\bar{1},0]=[\bar{1},1,0,0]$ in each period. It is thus obvious that the corresponding dislocation structure is completely different to that of a simple combination of **a** edge dislocations seen above for GaN.

By using the same procedure, the other Σ13 GB with rotation angle of 32.2° has been identified in the same sample. As shown in Fig. 5(a), along the boundary plane $\{\frac{1}{3}[\bar{2},7,\bar{5},0]/(\bar{4},1,3,0)\}$, side of the CSL, one may expect a Burgers vector of -2$\mathbf{a}_1$ as the dislocation content inside one period of boundary plane. The corresponding core structure has been determined to be the straight 5757-atom rings as shown in Fig. 6. We can see that, the dislocation core consists of two primitive dislocation elements (57-atom ring) with their Burgers vectors ($\mathbf{b}_1$ and $\mathbf{b}_2$) normal to the boundary plane. As seen for the boundary structure at the boundary plane $\{[\bar{3},4,\bar{1},0]/(\bar{5},\bar{2},7,0)\}$, diagonal of the CSL, in Fig. 5(a), a dislocation content of -2$\mathbf{a}_1$+2$\mathbf{a}_2$ is unveiled, which is two times larger than the case above of $[\bar{1},1,0,0]$. Correspondingly, two large white contrasts are exhibited in one period from the high-resolution TEM image. However, our determination is at variance with Carlsson et al. who reported a faceted 5757-atom rings as the structural unit for Σ13 32.2° GB [36,37]. Although this faceted 5757- configuration exhibits a $[1,0,\bar{1},0]$ Burgers vector, a close examination of the original experimental report [37] shows that the structure of this boundary may be much more complex. Therefore, the core structure of this $[1,0,\bar{1},0]$ edge dislocation in our observation should be subjected to more intimate examination.

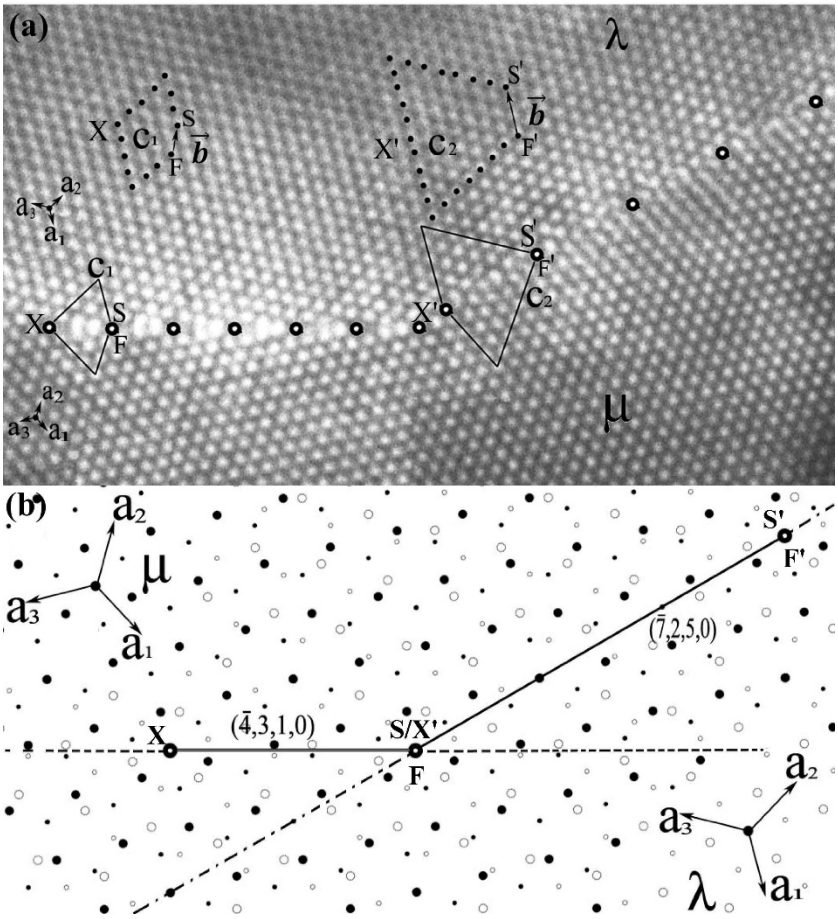

Fig. 4. (a) A high-resolution TEM micrograph of the Σ13 GB at the rotation angle of 27.8°. The defect contents for the side and diagonal of CSL are underlined by mapping the Burgers circuits: Burgers circuit C_1 corresponds to SXF circuit around boundary plane $\{\frac{1}{3}[2,5,\bar{7},0]/(\bar{4},3,1,0)\}$, side of the CSL, and in perfect λ crystal; Burgers circuit C_2 corresponds to S'X'F' circuit around boundary plane $\{[\bar{4},3,1,0]/(\bar{7},2,5,0)\}$, diagonal of the CSL, and in perfect λ crystal. Large open circles with their enclosed letters (X,S,F,X',S',F') indicate the boundary period, small black dots in TEM image show the Burgers circuit mapping. (b) The corresponding topological lay out in dichromatic complex showing the boundary planes and periods.

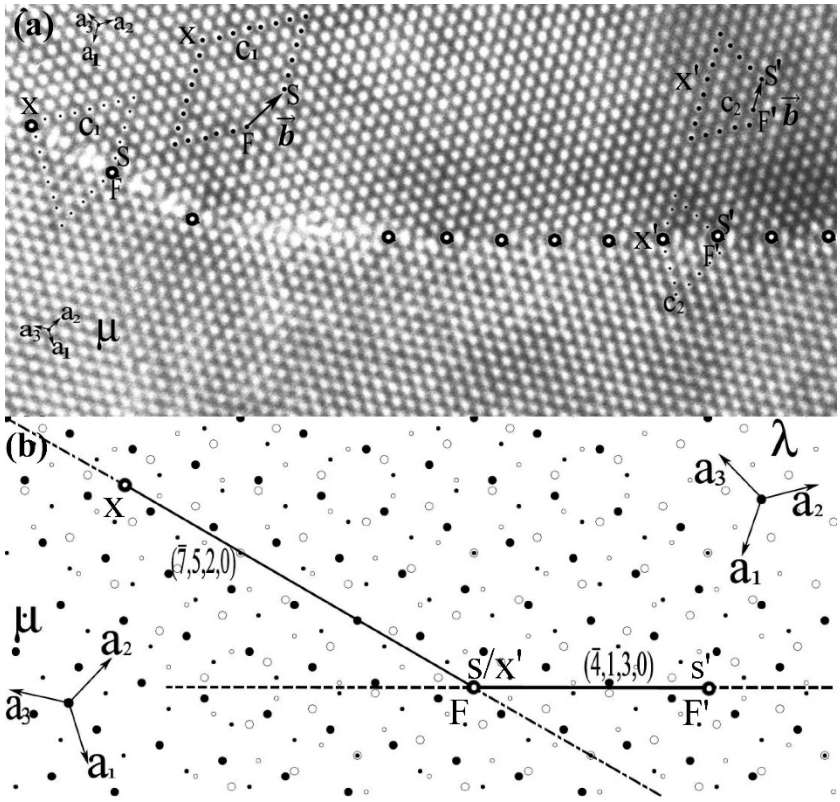

Fig. 5. (a) A HRTEM micrograph of the Σ13 32.2° GB. (b) The corresponding topological lay out in dichromatic complex showing the boundary planes and periods. The graphic representation follows the same way in Fig.4.

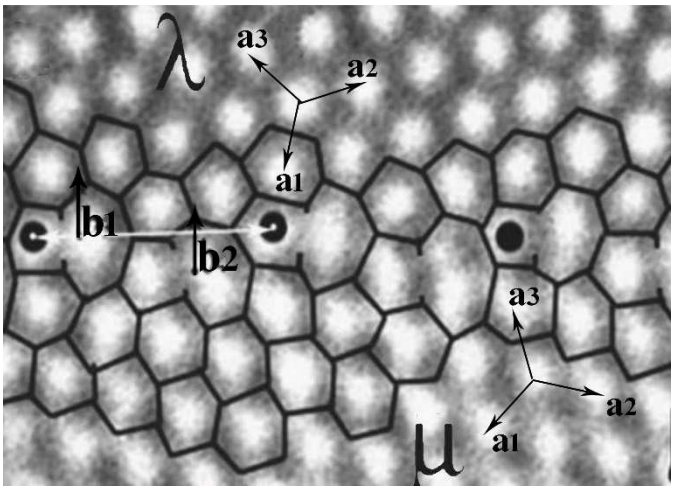

Fig. 6. Atom structure of Σ13 32.2° GB at boundary plane of $\{\frac{1}{3}[\bar{2},7,\bar{5},0]/(\bar{4},1,3,0)\}$. Atomic cycles are superimposed to show the periodicity, the Burgers vectors of the two primary dislocations one of each period are normal to boundary plane.

Table 3

Boundary structures of Σ13 27.8° [0001] tilt GB simulated using SW and SIESTA softwares. The energies are given in mJ/m^2.

Core Structure	Name	SW(O)	SW(C)	SIESTA	Burgers Vector (λ crystal)
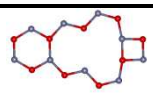	6684	1861	1861	1384	($\mathbf{a}_3$-$\mathbf{a}_1$)
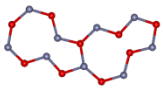	Faceted 5757	2481	1690	1694	($\mathbf{a}_3$-$\mathbf{a}_1$)
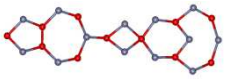	57468	1394	1304	1642	-3$\mathbf{a}_1$
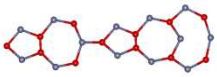	57578	1651	1619	1525	-3$\mathbf{a}_1$

Table 4

Boundary structures of Σ13 32.2° [0001] tilt GB simulated using SW and SIESTA softwares. The energies are given in mJ/m^2.

Core Structure	Name	SW(O)	SW(C)	SIESTA	Burgers Vector (λ crystal)
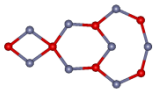	468	1177	1497	1364	-2$\mathbf{a}_1$
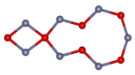	457	1609	2195	1367	-2$\mathbf{a}_1$
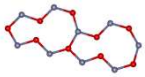	Straight 5757	2426	2000	1596	-2$\mathbf{a}_1$
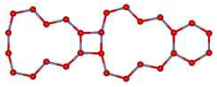	864866	1981	1981	1432	2($\mathbf{a}_3$-$\mathbf{a}_1$)

In order to determine this new structural unit of $[1,0,\bar{1},0]$ dislocation content, atomic simulation has been carried out using combinations of the known 4-, 8-, 57-, 6-atom rings and their mixtures. Table III and IV list the core structures of Σ13 GBs with relatively low formation energy, which should correspond to those that may be observed in experiments. The corresponding Burgers vectors are provided at the last column to show the defect contents: $\mathbf{a} = \frac{1}{3} < 11\bar{2}0 >$ or $[10\bar{1}0]$. As can be noticed, consistent with the energy tendency

calculated for the three basic structure units in Table II, core structures possessed 57-atom ring generally have high formation energy in both Table III and IV. However, the energy differences between the above atomic configurations of the cores are too small and it is difficult to conclude as for which of them could be the most stable, just through this theoretical modeling. In order to proceed further, extensive image simulations are implemented based on the proposed models to further identify the new core structure of $[10\bar{1}0]$ dislocation observed in Fig. 4 and Fig. 5.

The multislice technique in JEMS software was used in image simulations [26,27]. Depending on the minimum energy configuration shown in Table III and the Burgers vector content identified in Fig. 4, the 6684 large open core is seen to closely match with experimental observations. In Fig. 7(a) the periodic model of 6684 structural unit is presented. The Burgers circuit mapping in one period clearly exhibits a closure failure of ($\mathbf{a}_3$-$\mathbf{a}_1$), which corresponds to the observed dislocation content of $[10\bar{1}0]$. As seen in Fig. 7(b), the simulated image, under condition of the 5 nm thickness and 25 nm defocus value, shows one large white contrast connect with a normal one in right side, and with a quite small contrast on its left in one period. This is in agreement with the experimental micrograph shown in Fig. 7(c) where the periodic atom model is superimposed. In the model, the Zn-O bonds inside the dislocation core are vanished (pointed out by red dash line), which agrees with the large contrast observed by TEM. Coincidently, a fairly similar GB model with the 4-8-6 atom arrangement was also proposed by Oba et al. using both empirical potential and ab initio calculations [38]. They reported that, even this structure possesses dangling bonds, low formation energy of 1.42 J/m^2 was obtained resulting from the cooperative effects of bond distortion and dangling bond. This may confirm the rather low formation energy (1.384 J/m^2) in our SIESTA calculation tabulated in Table III. And also, they claimed that the electronic states near the band edges are not affected significantly by the structural deformation, which coincides with the behavior of 6684-core obtained from the DOS analysis presented below [38]. By far, the new open dislocation core observed in Σ13 27.8° GB has been identified as the structural unit made of connected 4-8-6 atom rings. As for the Σ13 32.2°×$\{[\bar{3},4,\bar{1},0]/(\bar{5},\bar{2},7,0)\}$ boundary plane which exhibits two large white contrasts in one period, the core structure can be considered as a long structural unit which comprises the same connected 4-8-6-atom rings in order to accommodate the large dislocation content amount of $2[\bar{1},1,0,0]$.

This close combination of TEM and topological CSL analysis completely reproduced the dislocation structural unit concept in both GaN and ZnO GBs. For GaN, boundary planes

exhibit only well separated $\mathbf{a} = \frac{1}{3} < 11\bar{2}0 >$ edge dislocations based on the three basic structural units: 4-, 8- and 57-atom rings. In this case, the Burgers vectors adapt their orientation in order to accommodate the rotation angles of GBs. In contrast, for ZnO, through the characterization of Σ13 (32.2°/27.8°) GBs, periodic boundary structures exhibiting a dislocation content of $[10\bar{1}0]$ are uncovered either in side or diagonal of the CSLs. And most interestingly, this new structural unit exhibit a large dislocation core with the connected 4-8-6 atom rings. Moreover this observed core perfectly agrees with the geometrical structure of $[10\bar{1}0]$ dislocation as proposed by Osipiyan and Smirinova [24] in their theoretical work on possible dislocations and jogs that may exist in the wurtzite symmetry materials.

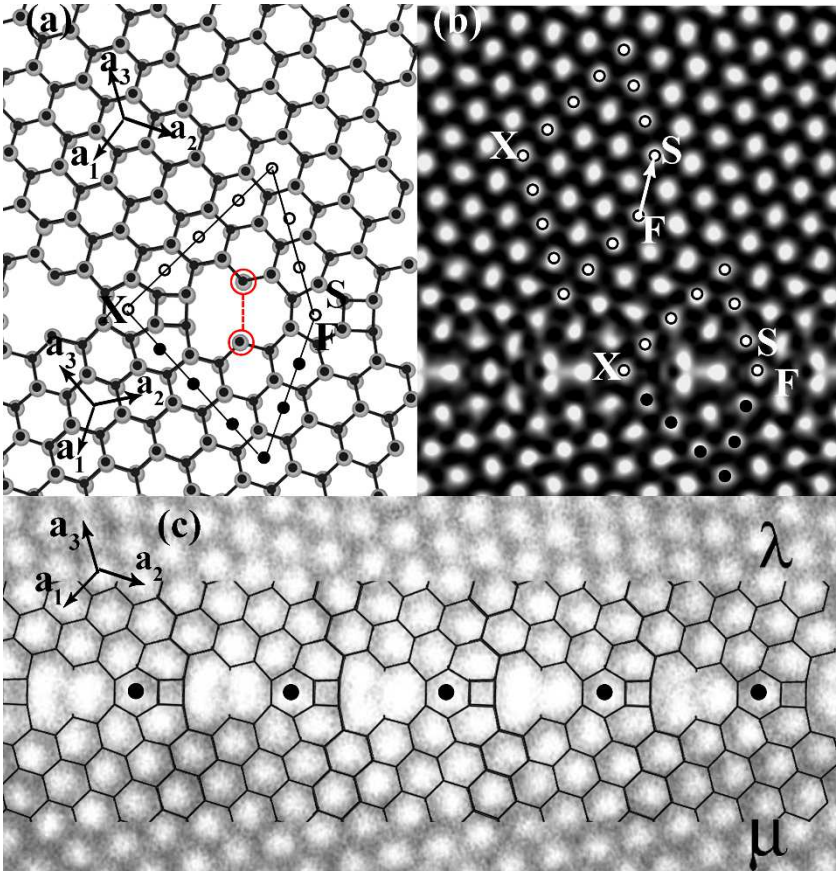

Fig. 7. Atomic structure of the Σ13 GB. (a) The periodic atom model of 6684 open core structure, and (b) the corresponding simulated image (defocus: 25 nm, thickness: 5 nm) showing the Burgers circuit SXF (($C_\lambda = 3\mathbf{a}_3 + 4\mathbf{a}_2$, $C_\mu = -4\mathbf{a}_3 - 3\mathbf{a}_1$). (c) High-resolution TEM micrograph of the Σ13 (27.8°)×$\{\frac{1}{3}[2,5,\bar{7},0]/(\bar{4},3,1,0)\}$ boundary plane. Four periods of dislocation content superimposed with the corresponding atomic model are shown.

5. Electronic structure

Apart from the topology and energetics, the influences of the GBs in ZnO and GaN related to electronic property are crucial for the practical applications [36]. Especially for the utilization of ZnO varistors, GB-induced deep acceptor levels formed below the bottom of conduction band maximum (CBM) can trap the electrons in bandgap, a double Schottky Barrier thus is build up resulting in the nonlinear current-voltage characteristics in devices [39,40]. The common concept ascribes this deep unoccupied electronic level to the GB itself and/or its cooperative effects with impurities and excessive oxygen [38]. However, the GB-induced deep donor electronic level formed above the VBM is also reported in the literature. For instance, Korner et al. [6] reported that the occupied deep levels above valence band edge originated from the undercoordinated O atoms in pure and/or non-stoichiometric ZnO GBs. Besides, local strain field in the vicinity of GBs is also considered to induce a deep state in some covalent compounds like GaN [41], Si, Ge and SiC, [38] in which the bond distortion is dominant.

In the present study, we have analyzed the electronic structures of those GBs proposed in Table III and IV, the corresponding total DOS are given in Fig. 8. For better visualization, the obtained DOS curves are artificially raised by 20-80 (1/eV) in order, with respect to the bulk one. As exhibited in Fig. 8, with SIC-LDA method, the band gap of ZnO is very well corrected to be 3.4 eV for bulk ZnO. For the ZnO GBs deal with in this study, the significant effects on the electronic states associated with GBs mainly appear at the valance band edges. Deep electronic levels are recognized above the VBM for configurations of faceted 5757, 57468 (seen in Fig. 8(a)) and straight 5757, 457 (shown in Fig. 8(b)), in which 57-atom ring is present. For the other configurations containing only 4-, 8- and perfect 6-atom rings, there is no additional contribution near the valence band edge. The obtained behavior in total DOS is consistent with the boundary energies calculated in Table III and IV showing that all 57-atom ring based configurations exhibit relatively high formation energies. It turns out that the 57-structure unit is the main factor to affect the system energy and contribute the electronic state inside the band gap. In the 57-structural unit core, a Zn atom faces to a Zn across the boundary plane, and so does O atom in next atom layer along [0001] direction. After structural relaxation, bond length population of Zn-Zn and O-O in 57-structural unit is implemented for all the 57-based GBs. It turns out that, the atom distance of Zn-Zn is about 1.34%-4.37% shorter than that of O-O inside these 57-structural units. This may suggest the coexistence of Zn-Zn wrong bond and oxygen dangling bond (O-O broken bond) in those boundary planes. In addition, an analysis of the local DOS for individual atom contribution

reveals that these deep electronic states come from the O dangling bonds in the boundaries. However, if we consider the 6684 core in which the undercoordinated O atoms are present, the Zn/O atom faces to another O/Zn atom across the boundary plane indicates that interfacial broken bonds is the normal Zn-O bonds rather than any wrong bond. In addition, its total DOS does not show any deep state near VBM. This study confirms that the GB-induced deep occupied states are not solely generated from the undercoordinated O atoms, it more likely comes from the cooperative effective of the established Zn-Zn wrong bond and O-O dangling bond (O-O broken). In contract, the total DOS at the bottom of conduction band are in general delocalized since the interaction of Zn:4s electrons are large in ZnO compound. Their shapes are slightly deviated to narrow the band gap for all the considered models. This seems to come from the structural deformation rise by the defective boundary regions. Indeed, our present results fairly agree with Oba et al [38], who reported bulklike electronic property for GBs only made by 4-, 8- and 6-atom rings. As seen in our results, deep state is not induced in those structures even for the GBs with dangling bonds like 6684, and 864866.

6. Conclusion

In summary, a detailed description using topological theory has been presented with a special focus on [0001] tilt Σ7 and Σ13 GBs. Combining high-resolution TEM and atomistic calculation, we demonstrate that GBs in GaN can be reconstructed using the three basic structural units of **a** edge dislocations. As for ZnO, a new structural unit is shown to possess the dislocation content of $[10\bar{1}0]$ in Σ13 GBs. The core structure is characterized as a compact mixture of 4-8-6-atom rings. The analysis electronic structure of the proposed GB structures indicate that the GB induced deep occupied state mainly originate from the complex interface ambient of established Zn-Zn wrong bond and O-O dangling bond in those 57-atom ring based GBs.

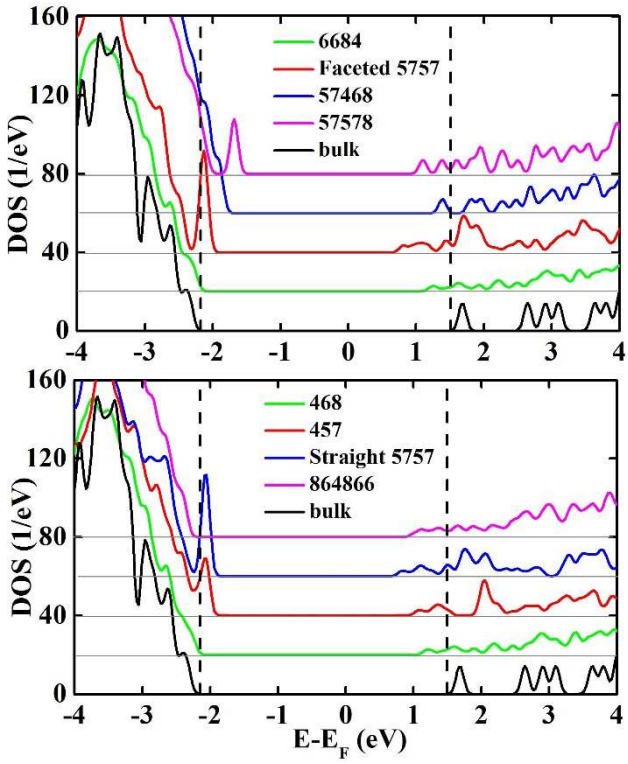

Fig. 8. Total DOS of the dislocation cores shown in table III and IV. The total DOS of bulk ZnO is given for comparison. Fermi level is specified to zero. The dashed lines in each figure indicates the valance band maximum and conduction band minimum positions.

Acknowledgement

The calculations have been carried through the computer resources of CRIANN "Centre Régional Informatique et d'Applications Numériques de Normandie" under project N° 2016009, which is gratefully acknowledged. Siqian Li is grateful to the China Scholarship Council for financial support under the file number 201508420147.

References

[1] L. Hozer and D. Holland, Semiconductor Ceramics: Grain Boundary Effects, Ellis Horwood, New York, 1994.

[2] G.H. Bishop and B. Chalmers, Dislocation structure and contrast in high angle grain boundaries, Philos. Mag. 24 (189) (1971) 515-526.

[3] M.J. Weins, H. Gleiter, B. Chalmers, Computer calculations of the structure and energy of high-angle grain boundaries, J. Appl. Phys. 42 (1971) 2639-2645.

[4] A.P. Sutton and V. Vitek, in Interfaces in Crystalline Materials, Oxford University Press, New York, 1995, pp: 286.

[5] V. Potin, P. Ruterana, G. Nouet, R.C. Pond, H. Morkoc, Mosaic growth of GaN on (0001) sapphire: A high-resolution electron microscopy and crystallographic study of threading dislocations from low-angle to high-angle grain boundaries, Phys. Rev. B 61 (2000) 5587-5599.

[6] W. Körner, C. Elsässer, First-principles density functional study of dopant elements at grain boundaries in ZnO, Phys. Rev. B 81 (2010) 08324.

[7] W. Körner, P.D. Bristowe, C. Elsasser, Density functional theory study of stoichiometric and nonstoichiometric ZnO grain boundaries, Phys. Rev. B 84 (2011) 045305.

[8] F. Oba, H. Ohta, Y. Sato, H. Hosono, T. Yamamoto, Y. Ikuhara, Atomic structure of [0001]-tilt grain boundaries in ZnO: A high-resolution TEM study of fiber-textured thin films, Phys. Rev. B 70 (2004) 125415.

[9] J. Chen, P. Ruterana, G. Nouet, Structural units and low-energy configurations of [0001] tilt grain boundaries in GaN, Phys. Rev. B 67 (2003) 205210.

[10] Y. Xin, S.J. Pennycook, N.D. Browning, P.D. Nellist, S. Sivanathan, F. Omnes, B. Beaumont, J.P. Faurie, P. Gibart, Direct observation of the core structures of threading dislocations in GaN, Appl. Phys. Lett. 72 (1998) 2680-2682.

[11] S. Ranganathan, On the geometry of coincidence-site lattices, Acta Cryst. 21 (1966) 197-199.

[12] P. Ruterana, G. Nouet, Atomic structure of extended defects in wurtzite GaN epitaxial layers, Phys. Stat. Sol. (b) 227 (2001) 177-228.

[13] L. Lymperakis, J. Neugebauer, M. Albrecht, T. Remmele, H.P. Strunk, Strain induced deep electronic states around threading dislocations in GaN, Phys. Rev. Lett. 93 (2004) 196401.

[14] F.A. Ponce, Defects and interfaces in GaN epitaxy, MRS Bulletin 22 (2) (1997) 51-57.

[15] P. Ruterana, V. Potin, B. Barbaray, G. Nouet, Growth defects in GaN layers on top of (0001) sapphire: A geometrical investigation of the misfit effect, Phil. Mag. A 80 (4) (2000) 937-954.

[16] V. Narayanan, K. Lorenz, W. Kim, S. Mahajan, Origins of threading dislocations in GaN epitaxial layers grown on sapphire by metalorganic chemical vapor deposition, Appl. Phys. Lett. 78 (2001) 1544-1546.

[17] P. Vermaut, P. Ruterana, G. Nouet, H. Morkoç, Microstructure of GaN epitaxially grown on hydrogen plasma cleaned 6H-SiC substrates, Inst. Phys. Conf. Ser. 146 (1995) 289.

[18] P. Ruterana, M. Abouzaid, A. Bere, J. Chen, Formation of a low energy grain boundary in ZnO: The structural unit concept in hexagonal symmetry materials, J. Appl. Phys. 103 (2008) 033501.

[19] R.C. Pond, D.S. Vlachavas, Bicrystallography, Proc. R. Soc. Lond. A 386 (1983) 95-143.

[20] R.C. Pond, N.A. McAuley, A. Serra, W.A.T. Clark, Transformation matrices for hexagonal and trigonal crystals, Scripta Met. 21 (1987) 197-202.

[21] A. Bere, A. Serra, Atomic structure of dislocation cores in GaN, Phys. Rev. B 65 (2002) 205323.

[22] R.C. Pond, On the characterisation of interfacial defects using high resolution electron microscopy, Interface Sci. 2 (1995) 299-310.

[23] J. Hornstra, Dislocations in the diamond lattice, J. Phys. Chem. Solids 5 (1958) 129-141.

[24] Y.A. Osipiyan, I.S. Smirnova, Perfect dislocations in the wurtzite lattice, Phys. Stat. sol. 30 (1968) 19-29.

[25] J. Chen, P. Ruterana, G. Nouet, The energy of tilt grain boundaries around <0001> in GaN, Phys. stat. sol. (a) 203 (2006) 247-258.

[26] P.A. Stadelmann. EMS - a software package for electron diffraction analysis and HREM image simulation in materials science, Ultramicroscopy 21 (1987) 131-145.

[27] P.A. Stadelmann, JEMS-EMS java version, 2004, Electron Microscopy Software, http://cimewww.epfl.ch/people/stadelmann/jemswebsite/jems.html.

[28] F.H. Stillinger, T.A. Weber, Computer simulation of local order in condensed phases of silicon, Phys. Rev. B 31 (1985) 5262-5271.

[29] N. Aïchoune, V. Potin, P. Ruterana, A. Hairie. G. Nouet, E. Paumier, An empirical potential for the calculation of the atomic structure of extended defects in wurtzite GaN, Comput. Mater. Sci. 17 (2000) 380-383.

[30] Y.F. Yan, M.M. Al-Jassim, Inversion domain boundaries in ZnO: First-principles total-energy calculations, Phys. Rev. B 69 (2004) 085204.

[31] J.M. Soler, E. Artacho, J.D. Gale, A. Garcia, J. Junquera, P. Ordejon, D. Sanchez-Portal, J. Phys.: Condens. Matter **14** (2002) 2745-2779.

[32] J.P. Perdew, A. Zunger, Self-interaction correction to density-functional approximations for many-electron systems, Phys. Rev. B 23 (1981) 5048-5079.

[33] J.E. Northrup, J. Neugebauer, L.T. Romano, Inversion Domain and Stacking Mismatch Boundaries in GaN, Phys. Rev. Lett. 77 (1996) 103-106.

[34] P. Ruterana, B. Barbaray, A. Béré, P. Vermaut, A. Hairie, E. Paumier, G. Nouet, A. Salvador, A. Botchkarev, H. Morkoc, Formation mechanism and relative stability of the

{$11\bar{2}0$} stacking fault atomic configurations in wurtzite (Al,Ga,In) nitrides, Phys. Rev. B 59 (1999) 15917-15925.

[35] J.Y. Roh, Y. Sato, Y. Ikuhara, Atomic structure of ZnO Σ13 [0001]/{$13\bar{4}0$} symmetric tilt grain boundary, J. Am. Ceram. Soc. 97 (2014) 617-621.

[36] J.M. Carlsson, H.S. Domingos, P.D. Bristowe, B. Hellsing, An Interfacial Complex in ZnO and Its Influence on Charge Transport, Phys. Rev. Lett. 91 (2003) 165506.

[37] A.N. Kiselev, F. Sarrazit, E.A. Stepantson, E. Olsson, T. Claeson, V.I. Bandarenko, R.C. Pond, N.A. Kiselev, High-resolution electron microscopy of ZnO grain boundaries in bicrystals obtained by the solid-phase intergrowth process, Philos. Mag. A 76 (1997) 633-655.

[38] F. Oba, S.R. Nishitani, H. Adachi, I. Tanaka, M. Kohyama, S. Tanaka, Ab initio study of symmetric tilt boundaries in ZnO, Phys. Rev. B 63 (2001) 045410.

[39] J.D. Russell, D.C. Halls, C. Leach, Grain boundary SEM conductive mode contrast effects in additive free zinc oxide ceramics, Acta Mater. 44 (1996) 2431-2436.

[40] D.R. Clarke, Varistor Ceramics, J. Am. Ceram. Soc. 82 (1999) 485-502.

[41] S.M. Lee, M.A. Belkhir, X.Y. Zhu, Y.H. Lee, Y.G. Hwang, T. Frauenheim, Electronic structures of GaN edge dislocations, Phys. Rev. B 61 (2000) 16033-16039.

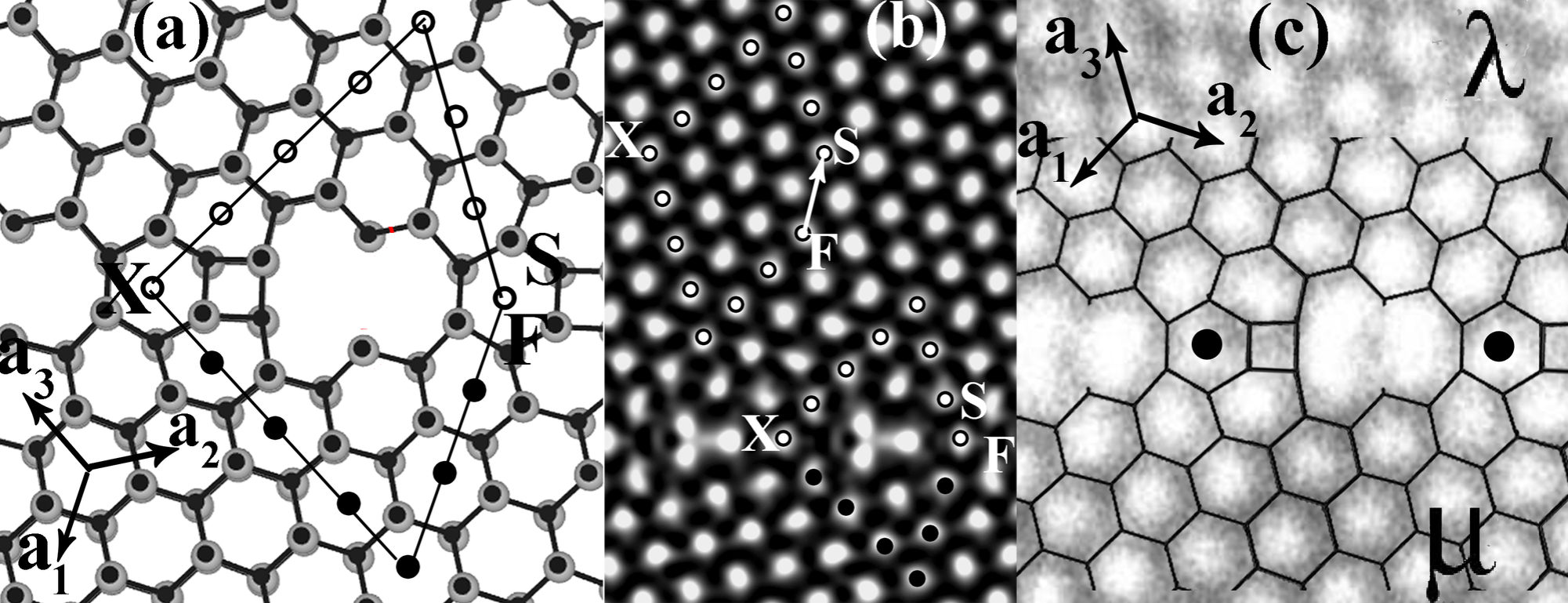
(a)
X
S
F
a3
a2
a1
(b)
X
S
F
X
S
F
(c)
a3
a2
a1
λ
μ